High resolution optical frequency domain reflectometry for characterization of components and assemblies

Brian J. Soller, Dawn K. Gifford, Matthew S. Wolfe and Mark E. Froggatt

Luna Technologies, 3157 State Street, Blacksburg, VA 24060

sollerb@lunatechnologies.com

Abstract: We describe a technique for polarization sensitive optical frequency domain reflectometry (OFDR) that achieves 22 micrometer two-point spatial resolution over 35 meters of optical length with -97 dB sensitivity in a single measurement taking only seconds. We demonstrate OFDR's versatility in both time- and frequency-domain metrology by analyzing a fiber Bragg grating (FBG) in both the spectral and impulse response domains. We also demonstrate how a polarization diversity receiver can be used in an OFDR system to track changes in the polarization state of light propagating through a birefringent component.

OCIS codes: (060.2920) Homodyning, (120.3180) Interferometry, (120.5050) Phase measurement, (230.1480) Bragg reflectors

References and links

1. W. Sorin and D. Baney, "Measurement of rayleigh backscatter at 1.55 μm with 32 μm spatial resolution," IEEE Photon. Technol. Lett. **4** 374-376 (1992).
2. J. P. Von der Weid, R. Passy, G. Mussi, and N. Gisin, "On the characterization of optical fiber network components with optical frequency domain reflectometry," J. Lightwave Tech. **15**, 1131–1141 (1997).
3. P. Oberson, B. Huttner, O. Guinnard, G. Ribordy, and N. Gisin, "Optical frequency domain reflectometry with a narrow linewidth fiber laser," IEEE Photon. Technol. Lett. **12** 867-869 (2000).
4. W. Eickhoff and R. Ulrich, "Optical frequency domain reflectometry in single-mode fiber," Appl. Phys. Lett. **39** 693–695 (1981).
5. U. Glombitza and E. Brinkmeyer, "Coherent frequency domain reflectomtry for charactization of single-mode integrated optical waveguides," J. Lightwave Technol. **11** 1377–1384 (1993).
6. M. Froggatt, T. Erdogan, J. Moore, and S. Shenk, "Optical frequency domain characterization (OFDC) of dispersion in optical fiber Bragg gratings," in *Bragg Gratings, Photosensitivity, and Poling in Glass Waveguides*, OSA Technical Digest Series (Optical Society of America, Washington, DC, 1999), paper FF2.
7. S. Kieckbusch, Ch. Knothe, and E. Brinkmeyer, "Fast and accurate characterization of fiber Bragg gratings with high spatial resolution and spectral resolution," in *Optical Fiber Communication*, OSA Technical Digest Series (Optical Society of America, Washington, DC, 2003), paper WL2.
8. G. D. VanWiggeren, A. R. Motamedi, B. Szafraniec, R. S. Tucker, and D. M. Baney, "Singe-scan polarization-resolved heterodyne optical network analyzer," in *Optical Fiber Communication*, OSA Technical Digest Series (Optical Society of America, Washington, DC, 2002), paper WK2.
9. M. Froggatt, "Distributed measurement of the complex modulation of a photoinduced Bragg grating in an optical fiber," Appl. Opt. **35** 5162–5164 (1996).
10. M. Froggatt and J. Moore, "High resolution strain measurement in optical fiber with Rayleigh scatter," Appl. Opt. **37**, 1735–1740 (1998).

#5817 - $15.00 US Received 19 November 2004; revised 20 January 2005; accepted 21 January 2005

11. S. H. Yun, G. J. Tearney, J. F. de Boer, N. Iftimia, and B. E. Bouma, "High-speed optical frequency-domain imaging," Opt. Express **11,** 2953–2963 (2003), http://www.opticsexpress.org/abstract.cfm?URI=OPEX-11-22-2953.
12. M. Wegmuller, M. Legre, and N. Gisin, "Distributed beatlength measurement in single-mode fibers with optical frequency-domain reflectometry," J. Lightwave Technol. **20** 828–835 (2002).
13. A. J. Rogers, "Polarization optical time-domain reflectometry", Electron. Lett. **16** 489–490 (1980).
14. M. E. Froggatt, B. J. Soller, D. G. Gifford and M. S. Wolfe, "Correlation and keying of rayleigh scatter for loss and temperature sensing in parallel optical netwroks," in *Optical Fiber Communication,* OSA Technical Digest Series (Optical Society of America, Washington, DC, 2004), paper PDP17.
15. J. Qian and W. Huang, "Coupled-mode theory for LP modes," J. Lightwave Technol. **4** 619–625 (1986).

1. Introduction

Optical reflectometry is a critical diagnostic tool for lightwave systems and components. There are basically three reflectometric techniques suitable for fiber-based applications: optical time domain reflectometry (OTDR), low coherence frequency domain reflectometry (OLCR) and coherent optical frequency domain reflectometry (OFDR). The different methods have trade-offs in range, resolution, speed, sensitivity and accuracy. Typically, the low coherence technique is used for sub-millimeter resolution measurements with very high sensitivity but only over limited range ($<$ 5 m)[1]. OTDR is used for longer range (several kilometers), low-resolution system-level applications.

OFDR falls between OTDR and OLCR in that its range capabilities are on the order of tens to hundreds of meters with millimeter-range resolution[2, 3]. OFDR is based on swept-wavelength homodyne interferometry[4, 5, 6]. Light from a tunable laser source (TLS) is split and sent through measurement and static reference arms of an interferometer and recombined at an optical detector. Interference fringes are generated as the laser frequency is tuned. Those fringes are detected and related to the optical amplitude and phase response of the system, or device under test (DUT). The interference fringes, occurring in the spectral domain of the DUT, data can be processed using the Fourier transform into the time domain. In the time domain, a map of the reflections as a function of length internal to the DUT can be constructed. Hence, OFDR can be used for both spectral and time domain reflectometry.

OFDR has advantages over OTDR and OLCR for certain applications. Specifically, the coherent technique is well-suited for applications that require a combination of high speed, sensitivity and resolution over intermediate length ranges. Applications that fall into this category include fiber-optic component and module characterization[2, 7, 8, 9], distributed optical sensing[10], and biomedical imaging[11].

Typically, OFDR systems designed to operate over intermediate length ranges (tens to hundreds of meters) lack the spatial resolution required for component-level metrology[3, 12]. In this report we describe a method for polarization diverse OFDR that achieves, to the best of our knowledge, the highest reported combination of length and resolution. Specifically, we describe an instrument for high-speed ($<$ 3 seconds) polarization-resolved measurements of fiber-optic assemblies with 22 μm spatial resolution (in glass) over 35 meters of optical length with -97 dB sensitivity. We show results for the reflectivity of a fiber Bragg grating (FBG) in the 1550 nm wavelength region in both the frequency and time domains. Further, we show that a polarization diversity detection technique can be used to track changes in the polarization state of light as a function of propagation length through a component. We use this technique to measure the beat length and thus the differential group index of refraction of a birefringent FBG.

2. Network layout

A detailed schematic of the optical network for polarization diverse coherent OFDR is shown below in Fig. 1. The optical system is comprised of a tunable laser source (TLS), two interferometers (one measurement and one trigger) and a polarization sensitive receiver. The receiver

#5817 - $15.00 US Received 19 November 2004; revised 20 January 2005; accepted 21 January 2005

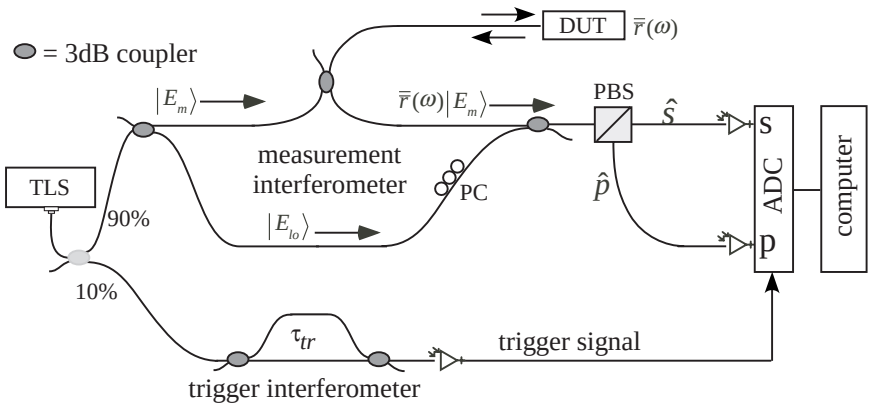

Fig. 1. Measurement network for polarization diverse OFDR. TLS = tunable laser source, ADC = analog to digital converter, PC = polarization controller, PBS = polarization beam splitter, and τ_{tr} = the differential time delay of the two paths in the trigger interferometer. Jones vectors are used to label the electric field at different locations in the network and the device under test is characterized by the complex spectral reflectivity, $\bar{\bar{r}}(\omega)$

includes a polarization beam splitter (PBS), three wide-band photodiodes, a high-speed analog to digital converter and a computer. Jones vectors are used to label the electric field at different locations in the network and the DUT is characterized by the complex spectral reflectivity, $\bar{\bar{r}}(\omega)$.

The PBS has the effect of splitting the reference field into two orthogonal states. This polarization diversity technique is used in OFDR to mitigate signal fading due to misalignment of the interfering measurement and local-oscillator fields. The addition of a polarizing element has the added benefit in OFDR [12] and OTDR [13] of allowing one to monitor changes in the state of polarization of the measurement field caused by the DUT.

When the laser frequency is tuned, interference fringes that can be related to the complex reflectivity of the DUT are observed at the detectors labeled '**s**' and '**p**'. Fringes from the trigger interferometer are used to trigger data acquisition at the **s** and **p** detectors. This well-known triggered-acquisition technique helps to mitigate tuning errors in the laser that would otherwise adversely affect the data[5].

Not shown is a portion of the network wherein a Hydrogen Cyanide gas-cell is used to monitor the instantaneous wavelength of the scanning laser. Hence, for a given scan, data is being taken simultaneously on four channels via the data acquisition card (DAQ).

The laser source used for these experiments was a Radians Pico model continuously tunable external cavity laser diode operating the C and L communication bands. The typical tuning range is from 2.5 nm to 40 nm centered at 1550 nm with a tuning rate of 20-80 nm/s, depending on the particular DUT. The laser tuning is controlled via analog voltage ramp generated using the DAQ card. The line-width of the laser used in these experiments is specified at 200 kHz and the operational output power used was 1 mW.

3. Theory and results

The amplitude of the measured interference fringes is proportional to the product of the interfering measurement and local-oscillator fields. We can write the field on the input side of the PBS at time '*t*' during the laser scan as the sum of the fields from the local oscillator, $|E_{lo}\rangle$, and

#5817 - $15.00 US Received 19 November 2004; revised 20 January 2005; accepted 21 January 2005

phase shifted measurement arm, $\bar{\bar{r}}(\omega)\,|E_m\rangle \exp[j\omega(t)\Delta\tau]$, of the measurement interferometer:

$$|E_{bs}\rangle = |E_{lo}\rangle + \bar{\bar{r}}(\omega)\,|E_m\rangle \exp[j\omega(t)\Delta\tau], \tag{1}$$

where $\bar{\bar{r}}(\omega)$ is the complex spectral reflectivity of the DUT, $\omega(t)$ is the instantaneous laser frequency and $\Delta\tau$ is the delay difference between the two arms of the measurement interferometer. We use dirac notation to represent the Jones vectors of the field in the fiber. The double-bar notation for the reflectivity represents the fact that in general, the reflectivity of a fiber coupled component or assembly is sensitive to the polarization state of the input electric field and can therefore be described by a two-by-two matrix (i.e. Jones matrix). This is equivalent to using a tensor to describe the complex coupling coefficient and hence the dielectric function of the DUT.

Using Eq. (1) and making the assumption that the current at the detector is proportional to the square of the electric field according to $i(\omega) \propto |\,|E_{bs}\rangle\,|^2$, we can write a simple form for the interference terms at the **s** and **p** detectors,

$$i_s(\omega) = 2\mathrm{Re}\left\{\langle E_{lo}|\,\bar{\bar{T}}_s^{\dagger}\bar{\bar{T}}_s\bar{\bar{r}}(\omega)\,|E_m\rangle \exp[j\omega(t)\Delta\tau]\right\}, \tag{2}$$

$$i_p(\omega) = 2\mathrm{Re}\left\{\langle E_{lo}|\,\bar{\bar{T}}_p^{\dagger}\bar{\bar{T}}_p\bar{\bar{r}}(\omega)\,|E_m\rangle \exp[j\omega(t)\Delta\tau]\right\}, \tag{3}$$

where $\bar{\bar{T}}_s$ and $\bar{\bar{T}}_p$ are projection operators that represent the splitting action of the beam splitter on the field in the fiber (eg. $\bar{\bar{T}}_s\,|E\rangle = E_s\hat{s}$). Note that terms that do not oscillate as a function of laser frequency have been dropped. Also, the coherence function of the laser has been left out of the description of the interference because it does not greatly affect the fringe visibility for the lengths under consideration in this report.

Information about the complex reflectivity of the DUT can be extracted from the interference described by Eqs. (2) and (3). The amplitude and phase of the reflectivity can be accessed directly in the spectral domain or they can be calculated in the time domain by use of a discrete Fourier transform. In the spectral domain, or frequency domain, the amplitude represents spectral return loss and the phase and its derivatives contain information about the length and dispersiveness of the DUT. In the time domain, the amplitude can be used to locate different reflective events within the DUT and the phase, or rather the phase derivative, can be related to the local wavelength of the reflective structure.

3.1. Calibration

The polarization diversity receiver must be balanced in order for the data to be properly calibrated. Ideally, the local oscillator field should be split evenly between the **s** and **p** states of the PBS. This is accomplished by blocking the light in the measurement path and adjusting the polarization controller while monitoring the dc power levels on the **s** and **p** detectors. The controller is adjusted such that there is an equal amount of power incident on each detector.

Reflectivity measurements can then be calibrated by measuring the magnitude of the reflectivity of a known strong reflector. We used a spectrally flat, gold-plated polished fiber termination with a nominal reflectivity of greater than 98%. All reflectivity values are then with respect to the reference value.

3.2. Frequency domain

Figure 2 shows the reflectivity and group delay (GD) of an FBG in reflection. These data were generated by digitizing the interference fringes associated with $i_s(\omega)$ and $i_p(\omega)$ in the frequency domain using a 12-bit, 5 mega-sample per second, four channel DAQ card. For triggered acquisition, the sampling frequency is determined by the laser sweep rate, γ, and the differential

#5817 - $15.00 US Received 19 November 2004; revised 20 January 2005; accepted 21 January 2005

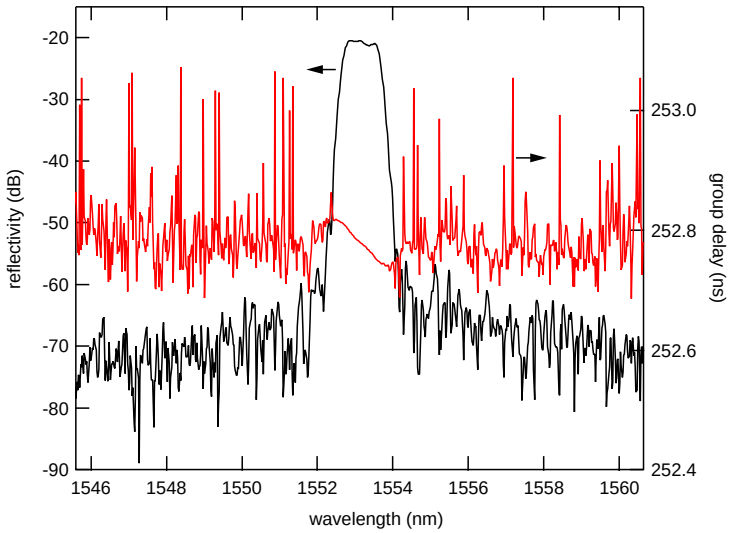

Fig. 2. Reflectivity (return loss) and group delay of a fiber Bragg grating.

delay in the auxiliary interferometer, τ_g, according to $f_s = \gamma\tau_g$. A laser sweep rate of 4.35 THz/s (35 nm/s) and an auxiliary interferometer delay of 800 ns were used to generate these data. This corresponds to a sampling frequency of $f_s = 3.48$ MHz. The corresponding wavelength resolution of the raw data sets is 0.01 pm, thus showing OFDR to be an extremely high-resolution technique.

The real-valued interference data is digitized in the frequency domain. A complex data set is generated in the frequency domain by (1) applying a discrete Fourier transform (DFT) to the real-valued data, (2) applying the appropriate window in the transform domain to extract the response of the DUT, and (3) transforming back to the frequency domain. This type of processing has the effect of down-sampling the resolution in the frequency domain. The data in Fig. 2 was down-sampled at an effective resolution of 1 pm.

The spectral reflectivity, $r(\omega)$, and GD, $\tau_g(\omega)$, are then calculated according to

$$r(\omega) = \sqrt{|i_s(\omega)|^2 + |i_p(\omega)|^2}, \tag{4}$$

$$\tau_g(\omega) = \frac{\angle\left\{i_s(\omega)i_s^*(\omega+\Delta\omega) + i_p(\omega)i_p^*(\omega+\Delta\omega)\right\}}{\Delta\omega}, \tag{5}$$

where $\Delta\omega$ is the effective frequency resolution and $\angle\{u\}$ denotes the phase of the complex data set u. Note the fidelity of the GD measurement in the -50 dB to -60 dB reflectivity range. Coherent detection enables this high sensitivity GD measurement. The GD outside of the passband of the grating becomes indeterminate due to the low reflectivity in the region (-60 dB to -90 dB).

3.3. Time domain

The coherent frequency domain technique was originally developed to measure reflections as a function of length in optical components. Often, optical component metrology requires spatial resolution in excess of 50 μm. Below we show that this spatial resolution can be achieved over measurement lengths exceeding 30 meters thus allowing for high speed, high resolution metrology of assemblies of components.

#5817 - $15.00 US Received 19 November 2004; revised 20 January 2005; accepted 21 January 2005

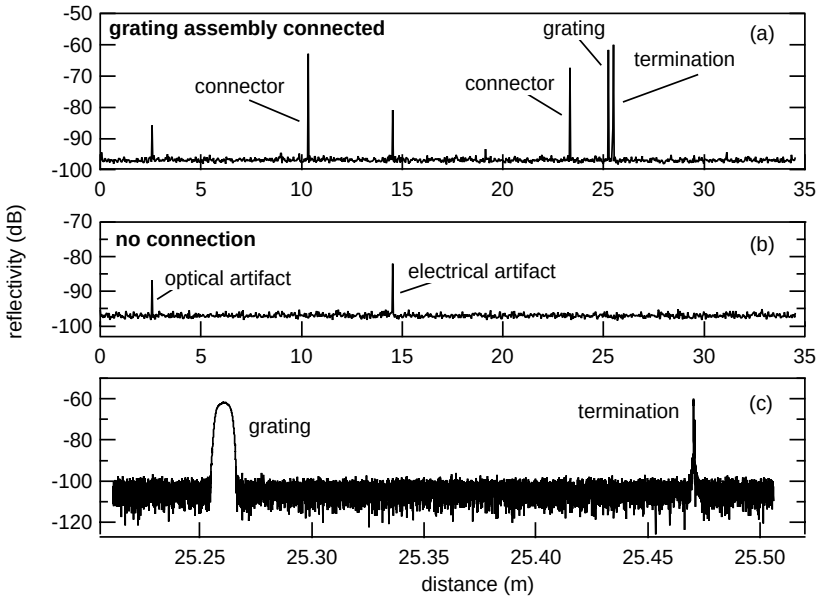

Fig. 3. (a) The reflectivity as a function of length of a 35 m optical assembly consisting of two fiber connectors and a fiber Bragg grating,(b) a reflectivity trace with no device connected, and (c) a blow up of the grating and fiber termination. These data were taken using a 40 nm wavelength scan centered at 1550 nm which corresponds to a resolution along the length axis of 20 μm. The time-synchronous electrical artifact in (b) is confirmed by taking data with no optical input.

The time domain representation of the data is given by the DFT of the raw data according to

$$\tilde{i}(\tau_k) = \sum_{n=0}^{N-1} i(\omega_n) \exp\left[-j\frac{2\pi kn}{N}\right], \tag{6}$$

where $\tilde{i}(\tau)$ is the time domain response of the DUT to the frequencies defined by the scan range in $i(\omega)$ and the subscripts denote the discrete nature of the data sets. Note that $i_s(\omega)$ and $i_p(\omega)$ must be transformed individually into $\tilde{i}_s(\tau)$ and $\tilde{i}_p(\tau)$. OTDR-like plots can be generated using the time-domain reflectivity: $r(\tau) = \sqrt{|\tilde{i}_s(\tau)|^2 + |\tilde{i}_p(\tau)|^2}$.

Figure 3(a) shows the time domain response of the grating assembly from Fig. 2. These data show clean reflectivity traces with identifiable reflection peaks over 35 m of optical length with -97 dB sensitivity. Figure 3(b) is the transform domain for a scan with no DUT connected and is shown for reasons of comparison. There are two measurement artifacts in the data: one due to an extra optical path in the system and one due to time synchronous clock noise in the acquisition electronics. The electrical contribution is confirmed by measuring the noise spectrum with no laser light present in the system. Figure 3(c) shows the portion of the assembly containing only the grating and the fiber termination. The time axis, τ, has been scaled to represent length using the group index of the fiber, $n_g = 1.48$, and the speed of light.

Noise effects in OFDR have been studied elsewhere[2] and we will not go into great detail here, but there are basically four contributions to the noise floor of -97 dB observed in Fig. 3. They are laser noise (intensity and phase), shot noise, thermal noise and amplifier noise. By process of elimination, we have determined that electrical noise in the amplifiers is dominat-

#5817 - $15.00 US Received 19 November 2004; revised 20 January 2005; accepted 21 January 2005

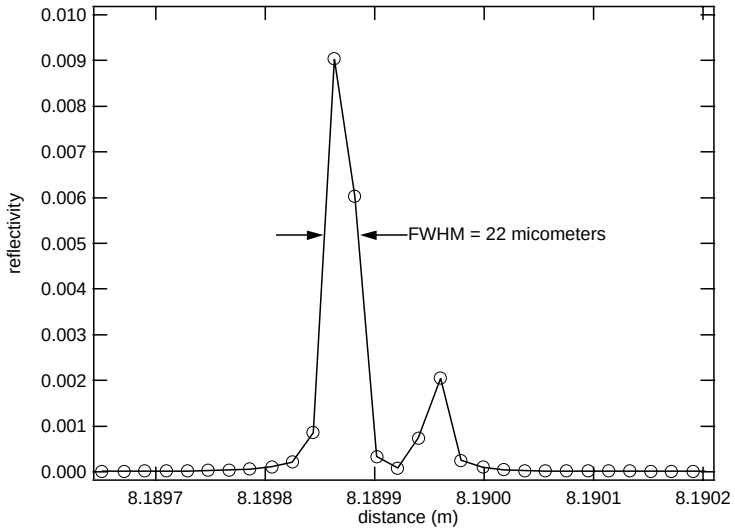

Fig. 4. The reflectivity on a linear scale of slightly mismatched, polished fiber (PC) terminations showing a 100 μm separation between the two fiber ends and 22 μm full width half maximum resolution of the individual peaks.

ing the -97 dB floor. Indeed our own investigations with "quieter" electronics have revealed Rayleigh-level sensitivities in a similar instrument[14].

The maximum DUT length of 35 m is determined by the differential delay in the trigger interferometer using the Nyquist sampling criteria by

$$L_{\max} = \frac{c\tau_g}{4n_g}, \tag{7}$$

where c is the speed of light in a vacuum, n_g is the group index of the DUT and the factor of four is due to the sampling theorem and the double-pass nature of the measurement interferometer. For an 800 ns differential delay, the maximum measurable DUT length is given by $L_{max} = 40$ m.

The spatial resolution of the measurement, Δz, is directly related to the resolution in the time domain and is determined by the spectral bandwidth of the scan range according to

$$\Delta z \cong \frac{c}{2n_g \Delta f}, \tag{8}$$

where $\Delta f \cong c\Delta\lambda/\lambda^2$. Equation (8) represents the minimum separation distance necessary to resolve two reflective events. This resolution can be corrupted by environmental noise, insufficiently linear laser tuning and and excess of unbalanced dispersion in the measurement arm. For our system, taking no special steps for temperature or vibration isolation, Eq. (8) holds and the corresponding maximum resolution for a 40 nm scan is 22 μm.

Figure 4 shows the reflectivity of two slightly mismatched fiber PC terminations and demonstrates the resolution of the OFDR measurement described here. The peaks in the data have a measured spatial separation of 100 μm and are clearly resolved. The measured resolution of the system based on the full-width-half-maximum of the individual reflectivity peaks is about 22 μm. It is important to note that this resolution is maintained over the entire 35 m of optical length.

#5817 - $15.00 US Received 19 November 2004; revised 20 January 2005; accepted 21 January 2005

The measurement time for the highest resolution scans over 35 m including laser scan time and data processing is about 5 seconds.

3.4. Polarization evolution

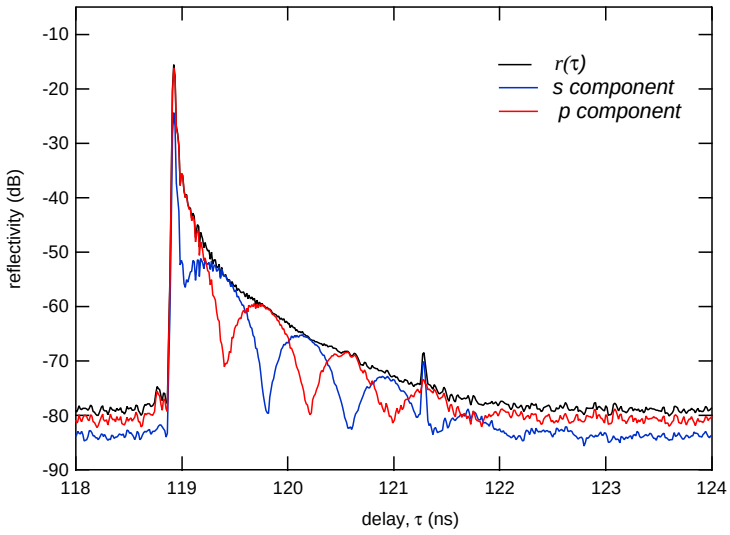

Fig. 5. The total reflectivity (black), and the reflectivity components recorded on the **s** and **p** detectors (blue and red) of a strong fiber Bragg grating. Beating in the **s** and **p** components represents birefringence in the grating and a rotation of the polarization state of the back-reflected light.

Birefringence can cause a change in the polarization state of the forward propagating and hence back-reflected light-wave in a given test sample or DUT. The interaction between the different propagating polarization modes can be described by vector coupled-wave analysis wherein the coupling coefficient is given by a tensor[15]. The tensor nature of the coupling coefficient for fiber-based devices leads directly to our description of the reflectivity using matrix notation.

The polarization diversity technique described here allows one to track changes in the state of polarization as the probe field propagates through the DUT. As the polarization state of the field reflected from the DUT changes, the polarization state of the light entering the PBS changes. This manifests as a change in the relative amplitudes of the interference fringes measured at the **s** and **p** detectors. By tracking separately the amplitudes of the DFTs of Eqs. (2) and (3), a picture of the polarization change as a function of propagation time (or distance) is formed.

Figure 5 shows the time domain reflectivity of a strong, birefringent grating. The **s** and **p** components of the total reflectivity are calculated from the amplitudes of the DFTs of $i_s(\omega)$ and $i_p(\omega)$ separately. The birefringent nature of the grating causes beating in the **s** and **p** components as the field propagates through the grating. The beat length can be extracted from these data by measuring the time over which one of the reflectivity components goes through one complete cycle.

The duration of the impulse response of the grating shown in Fig. 5 is about 2.8 ns, though it falls much faster to its half-width in about 12 ps (note the logarithmic scale). The propagation length in fiber corresponding to 2.8 ns of delay is about 0.6 m. This is much longer than the physical length of this grating (which is less than 1 cm). The apparent lengthening of the grating

#5817 - $15.00 US Received 19 November 2004; revised 20 January 2005; accepted 21 January 2005

is due to Fabry-Perot effects which cause light to make multiple round trips within the grating structure. The data in Fig. 5 have been smoothed using a box-car filter to an effective spatial resolution of 3 mm (15 ps) to show the slowly varying changes in the electric field polarization state over the course of multiple round trips through the grating.

An effective beat length for propagation in the grating of 0.16 m is established using $l_b = (c/2n_g)(1.6ns)$. The beat time of 1.6 ns is measured using Fig. 5 and we've used $n_g = 1.5$ as the average group index in the grating. The beat length can be converted to a index difference using $\Delta n = \lambda / l_b = 9.7x10^{(-6)}$. This is a very reasonable estimate of the birefringence in this type of grating structure.

4. Conclusion

Tunable laser-based OFDR has specific advantages over other fiber-based reflectometric techniques for metrology of components and systems on the order of tens to hundreds of meters of optical length. We have shown that availability of high fidelity tunable laser sources and modern computing and data acquisition products can extend the high-resolution capability of the technique out to cover distances over tens of meters. This enhanced range-(resolution) $^{(-1)}$ product is particularly useful for metrology of components that are already embedded in optical assemblies, components with long fiber pigtails, and for measuring multiple components simultaneously.

There are two ways to increase the length restriction of this instrument. One is to sample at a higher rate and the other is to decrease the laser tuning rate. Indeed OFDR systems with longer reach have been reported, though with lower resolution[3]. Our own investigations show that the technique described here can indeed be effective for lengths over 200 m with resolution in the 100 μm range.

The data presented here are single-scan in that no averaging was performed in producing them. This is a key element in the high-speed nature of the data acquisition and display. Further investigation using averaging to increase the measurement fidelity is currently underway.

We have employed FBGs in this paper as a canonical fiber-optic component with interesting characteristics in both the frequency and time domains. It should be noted that the technique described here is good for metrology of all fiber-coupled components that operate in the wavelength region of the tunable laser source.

Acknowledgments

The authors would like to thank Gary Miller at the Naval Research Laboratory and Turan Erdogan at Semrock Corporation for supplying the Bragg gratings.

#5817 - $15.00 US Received 19 November 2004; revised 20 January 2005; accepted 21 January 2005